Journal Name

ARTICLE TYPE

Cite this: DOI: 10.1039/xxxxxxxxxx

A computational protocol for the study of circularly polarized phosphorescence and circular dichroism in spin-forbidden absorption

Maciej Kamiński,[a] Janusz Cukras,[a,b] Magdalena Pecul,*[a] Antonio Rizzo[c] and Sonia Coriani*[b,d]

Received Date
Accepted Date

DOI: 10.1039/xxxxxxxxxx

www.rsc.org/journalname

We present a computational methodology to calculate the intensity of circular dichroism (CD) of spin-forbidden absorption and circularly polarized phosphorescence (CPP) signals, a manifestation of the optical activity of the triplet-singlet transitions in chiral compounds. The protocol is based on the response function formalism and is implemented at the level of time-dependent density functional theory. It has been employed to calculate the spin-forbidden circular dichroism and circularly polarized phosphorescence signals of valence $n \rightarrow \pi^*$ and $n \leftarrow \pi^*$ transitions, respectively, in several chiral enones and diketones. Basis set effects in the length and velocity gauge formulations have been explored, and the accuracy achieved when employing approximate (mean-field and effective nuclear charge) spin-orbit operators has been investigated. CPP is shown to be a sensitive probe of the triplet excited state structure. In many cases the sign of the spin-forbidden CD and CPP signals are opposite. For the β,γ-enones under investigation, where there are two minima on the lowest triplet excited state potential energy surface, each minimum exhibits a CPP signal of a different sign.

1 Introduction

Circularly polarized luminescence (CPL), the emission counterpart to electronic circular dichroism (ECD), measures the differential emission of left and right circularly polarized light by a chiral sample. CPL spectroscopy is far less widespread than ECD because of the difficulty of measurements, and, until recently, also because of the lack of quantum chemical calculations of the spectra, that could help in interpreting the experimental spectra. The latter obstacle has, however, recently been removed thanks to the development in time-dependent density-functional methods that allow to obtain excited state potential energy surface equilibrium structures as well as electric and magnetic dipole transition moments, necessary to evaluate the CPL intensities.[1,2] New developments have lately also occurred in experiment,[3] allowing to use CPL combined with quantum chemical calculations as a probe of the singlet excited state structure.[4,5]

Differential absorption and emission of left and right circularly polarized light take also place in spin-forbidden triplet-singlet transitions.[6,7] As far as emission is concerned, the resulting circularly polarized phosphorescence (CPP) was first measured long time ago,[6,7] but up to date no quantum chemical computational results of CPP have been reported, due to the lack of a computational protocol of the effect. However, the effect is very much of interest. Measurements of CPP have been recently reported together with the calculations of the associated excitation energies.[8,9] Circular dichroism in spin-forbidden absorption is being measured since at least early seventies,[10–12] but, as far as we know, it has never been calculated.

We found it worthwhile to derive the computational protocol and perform calculations of the CPP and spin-forbidden CD effect, especially since it opens up for the possibility of further studies of biologically relevant chromophores, considering that some of the transitions important in biochemistry are of triplet-singlet nature.[13,14]

The computational protocol, developed within a non-relativistic framework, is based on the concept that the intensity of circularly polarized phosphorescence can be obtained from the residues of appropriate quadratic response functions, in a parallel fashion to the phosphorescence lifetime.[15] It has been implemented within Time-Dependent Density Functional Theory (TD-DFT), as an extension of the existing code for phosphores-

[a] Faculty of Chemistry, University of Warsaw, Pasteura 1, 02-093 Warszawa, Poland.
[b] Dipartimento di Scienze Chimiche e Farmaceutiche, Università degli Studi di Trieste, via L. Giorgieri 1, I-34127 Trieste, Italy.
[c] Consiglio Nazionale delle Ricerche, Istituto per i Processi Chimico Fisici (IPCF-CNR), UOS di Pisa, I-56124 Pisa, Italy
[d] Aarhus Institute of Advanced Studies, Aarhus University, DK-8000 Aarhus C, Denmark
* Corresponding authors. E-mail: mpecul@chem.uw.edu.pl, coriani@units.it

cence lifetimes,[16] and it is applied to investigate CPP (and spin-forbidden ECD) in a series of chiral enones and diketones. Test calculations to check the basis set convergence and gauge-origin invariance were also carried out for hydrogen peroxide.

The selection of the systems to investigate is motivated by the possibility of using CPP as a probe of the structure of triplet excited states. The carbonyl group is flat in its ground state, whereas it puckers as a result of some of the excitations in the chromophore. For example, the equilibrium geometry of the singlet $\pi^* \leftarrow n$ excited state is no longer flat. The presence of another nearby chromophore, to which exciton coupling is possible (such as another carbonyl group or carbon-carbon double bond), has significant consequences for the shape of the CPL spectrum (probing the structure of the excited state) compared to that of the ECD spectrum (bearing signatures of the structure of the ground state). It has been demonstrated before for spin-allowed transitions, i.e. circularly polarized fluorescence,[2,17] that in certain enones the sign of the CPL signal of the band corresponding to the $\pi^* \rightarrow n$ transition is opposite to that of the ECD signal, corresponding to the $\pi^* \leftarrow n$ transition. The same may take place for the triplet-singlet $\pi^* \rightarrow n$ and $\pi^* \rightarrow \pi$ transitions.

In order to study this issue, we have calculated the CPL and CPP spectra for four out of five of the β,γ-enones studied in Ref. 2: (1S,3R)-4-methyleneadamantan-2-one (**1**), (1R,4R)-bicyclo[2.2.1]hept-5-en-2-one (**2**), (1R)-7-methylenebicyclo[2.2.1]heptan-2-one (**3**), and (1S)-2-methylenebicyclo[2.2.1]heptan-7-one (**4**). The most extended among the systems studied in Ref. 2, 1a-(1S,3R)-4-adamantylideneadamantan-2-one, is omitted, since the calculations of CPP are much more resource-consuming than those of CPL. On the other hand, we include in this study also an α,β-enone, namely the (R)-(−)4,4a,5,6,7,8-hexahydro-4a-methyl-2(3H)-naphthalenone (**5**), and two diketones: 1,7,7-trimethylbicyclo[2.2.1]heptane-2,3-dione (camphorquinone, **6**) and its isomer (1S,4R,5R)-5,7,7-trimethylbicyclo[2.2.1]heptane-2,3-dione (**7**) – as examples of ketones with conjugated double bonds. The structural formulae of the compounds under study are shown in Figure 1.

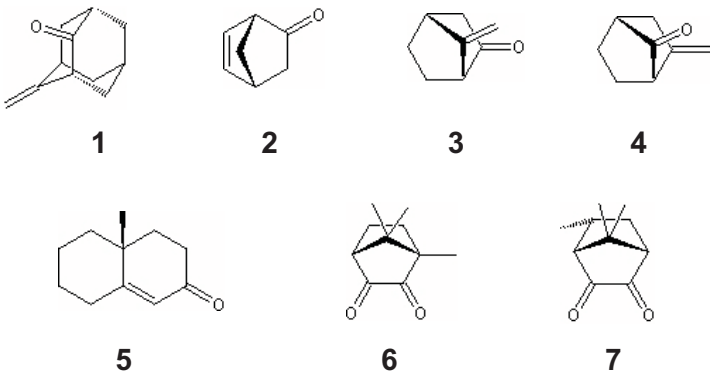

Fig. 1 The compounds under study:
(1S,3R)-4-methyleneadamantan-2-one (**1**),
(1R,4R)-bicyclo[2.2.1]hept-5-en-2-one (**2**),
(1R)-7-methylenebicyclo[2.2.1]heptan-2-one (**3**),
(1S)-2-methylenebicyclo[2.2.1]heptan-7-one (**4**),
(R)-(−)4,4a,5,6,7,8-hexahydro-4a-methyl-2(3H)-naphthalenone (**5**),
(1S,4R)-1,7,7-trimethylbicyclo[2.2.1]heptane-2,3-dione
(camphorquinone, **6**), (1S,4R,5R)-5,7,7
trimethylbicyclo[2.2.1]heptane-2,3-dione **7**

2 Theory

Our starting point to derive a computational protocol for circularly polarized phosphorescence is the consideration that the effect is, according to the experimental spectroscopists,[6] the "equivalent" of circularly polarized fluorescence for the case where the excited state is a triplet.

As shown in Ref. 2, spin-allowed CPL can be computed from the rotational strength of electronic circular dichroism, written, in length gauge, as

$$R^l_{|0^1f} = -\frac{\mathrm{i}e^2}{2m_e}\langle {}^1|0|\mathbf{r}|{}^1f\rangle \cdot \langle {}^1f|\mathbf{L}|{}^1|0\rangle \equiv -\frac{\mathrm{i}e^2}{2m_e}\langle {}^1|0|r_\alpha|{}^1f\rangle\langle {}^1f|L_\alpha|{}^1|0\rangle \quad (1)$$

and evaluated (in the Born-Oppenheimer approximation) at the optimized geometry of the excited state $|{}^1f\rangle$ (of the same multiplicity as the ground state), rather than at the ground state geometry, as otherwise done for conventional ECD. In the velocity-gauge formulation, the rotational strength of CPL can be expressed as

$$R^v_{|0^1f} = \frac{e^2}{2m_e^2\omega_{|_1f}}\langle {}^1|0|p_\alpha|{}^1f\rangle\langle {}^1f|L_\alpha|{}^1|0\rangle \quad (2)$$

with $\hbar\omega_{|_1f} = E_{|_1f} - E_{|_1|0}$.

Above, r_α, L_α, and p_α are Cartesian components of the (electronic) position, angular momentum and linear momentum operators, respectively. Einstein's implicit summation over repeated indices is assumed here and throughout.

In linear response theory,[18] the scalar rotatory strength is calculated as a residue of the linear response function[19]

$$\begin{aligned} R^l_{|0^1f} &= -\frac{\mathrm{i}e^2}{2m_e}\left\langle {}^1|0|r_\alpha|{}^1f\right\rangle\left\langle {}^1f|L_\alpha|{}^1|0\right\rangle \\ &= -\frac{\mathrm{i}\hbar e^2}{2m_e}\lim_{\omega\to\omega_{|_1f}}\left(\omega-\omega_{|_1f}\right)\langle\langle r_\alpha;L_\alpha\rangle\rangle_\omega\,, \end{aligned} \quad (3)$$

$$\begin{aligned} R^v_{|0^1f} &= \frac{e^2}{2m_e^2\omega_{|_1f}}\left\langle {}^1|0|p_\alpha|{}^1f\right\rangle\left\langle {}^1f|L_\alpha|{}^1|0\right\rangle \\ &= \frac{\hbar e^2}{2m_e^2\omega_{|_1f}}\lim_{\omega\to\omega_{|_1f}}\left(\omega-\omega_{|_1f}\right)\langle\langle p_\alpha;L_\alpha\rangle\rangle_\omega\,. \end{aligned} \quad (4)$$

To obtain the CPP analogue, we need to derive an expression for the rotational strength where the excited state is a triplet state $|{}^3f\rangle$ (assuming that the molecule is closed-shell and that the ground state, denoted now as $|{}^1|0\rangle$, is a singlet),

$$R^l_{|0^3f} = -\frac{\mathrm{i}e^2}{2m_e}\langle {}^1|0|r_\alpha|{}^3f\rangle\langle {}^3f|L_\alpha|{}^1|0\rangle, \quad (5)$$

$$R^v_{|0^3f} = \frac{e^2}{2m_e^2\omega_{|_3f}}\langle {}^1|0|p_\alpha|{}^3f\rangle\langle {}^3f|L_\alpha|{}^1|0\rangle\,. \quad (6)$$

with $\hbar\omega_{|_3f} = E_{|_3f} - E_{|_1|0}$. If evaluated at the ground state geometry, the above rotational strengths give the ECD intensity originating

from the singlet to triplet transition in absorption. If evaluated at the equilibrium geometry of the triplet excited state, on the other hand, they yield the difference of intensity of left- and right circularly polarized light originating from the triplet to singlet emission process—that is, the intensity of CPP.

The transition moments between a singlet state and a triplet state are obtained directly from the residue of the linear response function when relativistic two- or four-component wave functions are used,[20,21] whereas this is not the case for non-relativistic theories, as such transitions are spin-forbidden. However, in the non-relativistic case and within a perturbation theory framework, these dipole transitions become allowed when spin-orbit-perturbed ground and excited-state wave functions are introduced.[15] At first-order the electric dipole transition moment can be written as[15]

$$\begin{aligned}\langle {}^1 0|r_\alpha|{}^3 f\rangle^{(1)} &= \langle {}^1 0^{(0)} + {}^3 0^{(1)}|r_\alpha|{}^1 f^{(1)} + {}^3 f^{(0)}\rangle \\ &= \langle {}^1 0^{(0)}|r_\alpha|{}^1 f^{(1)}\rangle + \langle {}^3 0^{(1)}|r_\alpha|{}^3 f^{(0)}\rangle\end{aligned} \tag{7}$$

where superscripts (0) and (1) label zeroth- and first-order contributions within the perturbative expansion.

Considering a basis of unperturbed singlet and triplet states, the first-order spin contaminants of the ground and excited states can be written as[15]

$$|{}^3 0^{(1)}\rangle = \frac{1}{\hbar}\sum_{{}^3 k} \frac{|{}^3 k^{(0)}\rangle\langle {}^3 k^{(0)}|H_{so}|{}^1 0^{(0)}\rangle}{\omega_{{}^3 k}} \tag{8}$$

$$|{}^1 f^{(1)}\rangle = \frac{1}{\hbar}\sum_{{}^1 k} \frac{|{}^1 k^{(0)}\rangle\langle {}^1 k^{(0)}|H_{so}|{}^3 f^{(0)}\rangle}{\omega_{{}^1 f} - \omega_{{}^1 k}} \tag{9}$$

In these equations the spin-orbit operator H_{so}, given by[22]

$$\begin{aligned}H_{so} &= \frac{e^2\hbar g_e \alpha^2}{16\pi\varepsilon_0 m_e^2}\left[\sum_{iA} Z_A \frac{\mathbf{L}_{iA}\cdot\mathbf{s}_i}{r_{iA}^3} - \sum_{ij}\frac{\mathbf{L}_{ij}\cdot(\mathbf{s}_i + 2\mathbf{s}_j)}{r_{ij}^3}\right] \\ &\equiv \sum_i H_{so,1}(i) + \sum_{ij} H_{so,2}(i,j)\end{aligned} \tag{10}$$

is introduced. The indices i and j refer to the electrons, A to the nuclei, $\mathbf{r}_{ij}$ is the position of particle i relative to particle j, $\mathbf{L}_{ij} = \mathbf{r}_{ij}\times\mathbf{p}_i$ is the orbital angular momentum of particle i, of spin $\mathbf{s}_i$, with respect to the position of particle j, Z_A is the charge of nucleus A, g_e is the electron g factor and α is the fine-structure constant. $H_{so,1}(i)$ and $H_{so,2}(i,j)$ denote the one- and two-electron parts of the spin-orbit operator, respectively.

Inserting the first-order corrections Eqs. (8) and (9) into the expression for the transition moments, the first-order contribution to the dipole transition moment between singlet and triplet states is shown to be written as

$$\langle {}^1 0|r_\alpha|{}^3 f\rangle^{(1)} = \frac{1}{\hbar}\sum_{{}^1 k}\frac{\langle {}^1 0|r_\alpha|{}^1 k\rangle\langle {}^1 k|H_{so}|{}^3 f\rangle}{\omega_{{}^1 k} - \omega_{{}^3 f}} + \frac{1}{\hbar}\sum_{{}^3 k}\frac{\langle {}^1 0|H_{so}|{}^3 k\rangle\langle {}^3 k|r_\alpha|{}^3 f\rangle}{\omega_{{}^3 k}} \tag{11}$$

which is obtainable from the single residue of an appropriate quadratic response function[15]

$$\langle {}^1 0|r_\alpha|{}^3 f\rangle^{(1)} \Leftarrow \hbar \lim_{\omega\to\omega_{{}^3 f}} (\omega - \omega_{{}^3 f})\langle\langle r_\alpha; H_{so}, V^\omega\rangle\rangle_{0,\omega} \tag{12}$$

where V^ω is an arbitrary triplet operator (that determines the excitation vector) and $\hbar\omega$ matches the singlet-to-triplet excitation energy. An analogous relationship holds for the angular momentum transition moment

$$\begin{aligned}\langle {}^1 0|L_\alpha|{}^3 f\rangle^{(1)} &= \frac{1}{\hbar}\sum_{{}^1 k}\frac{\langle {}^1 0|L_\alpha|{}^1 k\rangle\langle {}^1 k|H_{so}|{}^3 f\rangle}{\omega_{{}^1 k} - \omega_{{}^3 f}} + \frac{1}{\hbar}\sum_{{}^3 k}\frac{\langle {}^1 0|H_{so}|{}^3 k\rangle\langle {}^3 k|L_\alpha|{}^3 f\rangle}{\omega_{{}^3 f}} \\ &\Leftarrow \hbar \lim_{\omega\to\omega_{{}^3 f}} (\omega - \omega_{{}^3 f})\langle\langle L_\alpha; H_{so}, V^\omega\rangle\rangle_{0,\omega}\end{aligned} \tag{13}$$

Thus, alike the phosphorescence dipole strength (and transition rate) from excited state $|{}^3 f\rangle$, that can be obtained as the square of the phosphorescence transition matrix element

$$\begin{aligned}D^l_{{}^1 0{}^3 f} &= e^2\langle {}^1 0|r_\alpha|{}^3 f\rangle\langle {}^3 f|r_\alpha|{}^1 0\rangle \\ &\Leftarrow e^2\hbar^2\left[\lim_{\omega\to\omega_{{}^3 f}} (\omega - \omega_{{}^3 f})\langle\langle r_\alpha; H_{so}, V^\omega\rangle\rangle_{0,\omega}\right]^2,\end{aligned} \tag{14}$$

$$\begin{aligned}D^v_{{}^1 0{}^3 f} &= \frac{e^2}{m_e^2\omega_{{}^3 f}^2}\langle {}^1 0|p_\alpha|{}^3 f\rangle\langle {}^3 f|p_\alpha|{}^1 0\rangle \\ &\Leftarrow \frac{\hbar^2 e^2}{m_e^2\omega_{{}^3 f}^2}\left[\lim_{\omega\to\omega_{{}^3 f}} (\omega - \omega_{{}^3 f})\langle\langle p_\alpha; H_{so}, V^\omega\rangle\rangle_{0,\omega}\right]^2,\end{aligned} \tag{15}$$

the rotational strength of circularly polarized phosphorescence is computed from the residues

$$\begin{aligned}R^l_{{}^1 0{}^3 f} &= -\frac{\mathrm{i}e^2}{2\hbar^2 m_e}\left[\sum_{{}^1 k}\frac{\langle {}^1 0|r_\alpha|{}^1 k\rangle\langle {}^1 k|H_{so}|{}^3 f\rangle}{\omega_{{}^1 k} - \omega_{{}^3 f}} + \sum_{{}^3 k}\frac{\langle {}^1 0|H_{so}|{}^3 k\rangle\langle {}^3 k|r_\alpha|{}^3 f\rangle}{\omega_{{}^3 k}}\right] \\ &\quad\times\left[\sum_{{}^1 k}\frac{\langle {}^1 0|L_\alpha|{}^1 k\rangle\langle {}^1 k|H_{so}|{}^3 f\rangle}{\omega_{{}^1 k} - \omega_{{}^3 f}} + \sum_{{}^3 k}\frac{\langle {}^1 0|H_{so}|{}^3 k\rangle\langle {}^3 k|L_\alpha|{}^3 f\rangle}{\omega_{{}^1 k}}\right]^\dagger \\ &\Leftarrow -\frac{\mathrm{i}\hbar^2 e^2}{2m_e}\left(\lim_{\omega\to\omega_{{}^3 f}} (\omega - \omega_{{}^3 f})\langle\langle r_\alpha; H_{so}, V^\omega\rangle\rangle_{0,\omega}\right) \\ &\quad\times\left(\lim_{\omega\to\omega_{{}^3 f}} (\omega - \omega_{{}^3 f})\langle\langle L_\alpha; H_{so}, V^\omega\rangle\rangle_{0,\omega}\right)^\dagger\end{aligned} \tag{16}$$

in the length gauge, and as

$$\begin{aligned}R^v_{{}^1 0{}^3 f} &\Leftarrow \frac{\hbar^2 e^2}{2m_e^2\omega_{{}^3 f}}\left(\lim_{\omega\to\omega_{{}^3 f}} (\omega - \omega_{{}^3 f})\langle\langle p_\alpha; H_{so}, V^\omega\rangle\rangle_{0,\omega}\right) \\ &\quad\times\left(\lim_{\omega\to\omega_{{}^3 f}} (\omega - \omega_{{}^3 f})\langle\langle L_\alpha; H_{so}, V^\omega\rangle\rangle_{0,\omega}\right)^\dagger\end{aligned} \tag{17}$$

in the velocity gauge. In Eqs. (12)-(17) above we used the symbol "⇐" instead of an equality sign to underline the fact that the complete single residue of the given quadratic response functions is the product of a "two-photon"-like transition moment [see the SOS expressions given in Eqs. (11), (13) and (16)] with a "one-

photon" transition moment [e.g., $\langle^3 f|V^{\omega}|0\rangle$], whereas the CPP and phosphorescence transition strenghts/moments only correspond to the "two-photon" part of the single residues.

Since the spin-orbit operator is a two-electron operator, the calculation of phosphorescence (and circularly-polarized phosphorescence) intensities becomes time consuming. The full spin-orbit operator as given in Eq. (10) can be replaced by effective one-electron operators, [23–25] see also Ref. 26 for a detailed discussion of the differences in these approximate spin-orbit operators. Here, we have set up the computation of the CPP employing the Atomic Mean-Field spin-orbit operator,[23,24] H_{so}^{AMFI}, which exploits the AMFI integral code by Schimmelpfennig.[27] In the atomic mean field the matrix elements between two Slater determinants differing by a single valence spin orbital excitation are given by

$$H_{so,ij}^{\mathrm{AMFI}} = \langle i|H_{so,1}(1)|j\rangle + \frac{1}{2}\sum_{k,\mathrm{fixed}\,n_k} n_k \left[\langle ik|H_{so,2}(1,2)|jk\rangle - \langle ik|H_{so,2}(1,2)|kj\rangle - \langle ki|H_{so,2}(1,2)|jk\rangle\right] \quad (18)$$

where the occupation numbers n_k are fixed, and the two-electron terms of Eq. (10) are summed in a way analogous to the two-electron terms in the Fock operator. We also considered the effective nuclear charge spin-orbit H_{so}^{EC} approximation to the spin-orbit operator[25,28]

$$H_{so}^{\mathrm{EC}} \approx \frac{e^2\hbar g_e \alpha^2}{16\pi\varepsilon_0 m_e^2}\sum_{i,A} Z_{\mathrm{eff}}(A)\frac{\mathbf{L}_{iA}\cdot\mathbf{s}_i}{r_{iA}^3} \quad (19)$$

where all two-electron terms in Eq. (10) are neglected, and compensated for by introducing a semi-empirical parameter, namely the effective nuclear charge (Z_{eff}), in place of Z_A in the one-electron term.

3 Computational details

Unless noted otherwise, the transition moments were calculated using the Coulomb-attenuated Becke 3-Parameter (Exchange), Lee, Yang and Parr functional (CAM-B3LYP) functional[29] with the aug-cc-pVDZ[30–33] basis set. The geometries were optimized using CAM-B3LYP (as implemented in Gaussian 09) with the cc-pVDZ basis set. A pre-release version of Dalton 2015[34,35] was used for the calculations of the rotational strengths. Gauge origin has been placed in the centre of mass, except for one set of test calculations for H_2O_2.

The calculations for hydrogen peroxide have been carried out for the ground-state structure (with geometry parameters taken from Ref. 36), since the molecule is flat (and therefore non-chiral) in its low-lying triplet excited states.[37] The results we report for this molecule correspond therefore to spin-forbidden circular dichroism rather than circularly polarized phosphorescence.

The scaling factors for the effective nuclear charges entering the H_{so}^{EC} operator in the Dalton program are taken from Ref. 25.

4 Results

4.1 Basis set convergence of CPP intensity in length gauge and velocity gauge formulation

Prior to exploring possible applications of CPP for structural studies of triplet excited states of ketones, we discuss its dependence on the size and quality of the basis set, and compare the performance of the length and velocity gauge formulations. Test calculations have been carried out for H_2O_2 and for the enone **5**. The results are shown in Table 1 and Table 2, respectively.

Table 1 Comparison of the velocity (D^v, R^v) and length (D^l, R^l) gauge results for the dipole [10^{-40} esu^2 cm^2] and rotational [10^{-40} esu cm erg G^{-1}] strengths of the spin-forbidden HOMO-LUMO transition in H_2O_2, calculated with the full two-electron spin-orbit operator, Eq. 10, and different basis sets. The dipole strengths determine the intensity of the spin-forbidden absorption, and the rotational strengths of the spin-forbidden ECD. CAM-B3LYP results.

Basis set	# functions	D^l	D^v	$R^l \times 10^2$	$R^v \times 10^2$
aug-cc-pVDZ	64	3.58	2.85	−1.44	−1.52
aug-cc-pVTZ	138	3.66	3.60	−1.47	−1.48
aug-cc-pVQZ	252	3.71	3.57	−1.49	−1.47
d-aug-cc-pVDZ	90	3.61	3.98	−1.48	−1.59
d-aug-cc-pVTZ	188	3.70	3.68	−1.49	−1.51
d-aug-cc-pVQZ	334	3.74	3.63	−1.51	−1.49
aug-cc-pCVDZ	72	3.93	4.34	−1.59	−1.70
aug-cc-pCVTZ	164	3.86	3.71	−1.56	−1.53
aug-cc-pCVQZ	310	3.78	3.64	−1.52	−1.50

In general, the calculated rotational strengths, characterizing the CPP intensity, are fairly robust with respect to the basis set size. Both the rotational and the dipole strengths of the enone **1** are more sensitive to the basis set size than those of H_2O_2 (in particular the dipole ones), but even there the aug-cc-pVDZ basis set reproduces correctly the sign and the order of magnitude of the effect. Double augmentation improves slightly the results, while addition of tight core functions does not seem to have any beneficial effect. However, it should be mentioned at this point that the triplet excited states under study are valence states (π^* in ketones, and π^*, σ^* in H_2O_2), with small Rydberg character.[37] As observed for the rotational strength of spin-allowed transitions,[38] Rydberg states are likely to be much more demanding with respect to basis set requirements, and the addition of a larger number of diffuse functions may then be advisable when treating that type of states.

As expected, the difference between the dipole strengths and the rotational strengths calculated according to the length and velocity gauge formalism decreases when the basis set size increases. The convergence of the two sets of results towards each other is nevertheless slow. The percentage difference between the length and the velocity gauge results is larger for the dipole than for the rotational strength. This is not too surprising, given that the dipole operator enters squared in the former. For the rotational strength, the percentage difference does not exceed 10% even for the smallest basis set. The velocity gauge results converge faster with the basis set size than the length-gauge ones. Based on this evidence, in the following sections only the former

Table 2 The dipole [10^{-40} esu^2 cm^2] and rotational [10^{-40} esu cm erg G^{-1}] strengths of enone **5** corresponding to the transition to (absorption, ground-state geometry) and from (emission, excited-state geometry) the T1 excited state, calculated in the length and velocity gauges. CAM-B3LYP results.

	Absorption		Emission	
Basis	Length	Velocity	Length	Velocity
	Dipole strength, D			
aug-cc-pVDZ	$2.22{\cdot}10^{-1}$	$2.13{\cdot}10^{-1}$	7.70	7.52
daug-cc-pVDZ	$2.25{\cdot}10^{-1}$	$2.19{\cdot}10^{-1}$	7.67	7.52
aug-cc-pVTZ	$1.69{\cdot}10^{-1}$	$1.66{\cdot}10^{-1}$	8.59	8.56
	Rotational strength, $R \times 10^3$			
aug-cc-pVDZ	−3.46	−3.37	4.33	4.31
daug-cc-pVDZ	−3.49	−3.42	4.32	4.31
aug-cc-pVTZ	−3.07	−3.05	4.73	4.71

are discussed.

Further advantage of the velocity gauge over the length gauge formulation is that the rotatory strength calculated using the former is supposed to be independent of the choice of the gauge origin for the vector potential of the magnetic field. We have verified this by carrying out two sets of calculations for H_2O_2: one with the gauge origin placed, as default, in the centre of mass, and a second set of calculations with the origin moved away with respect to the centre of mass by the (a_0, a_0, a_0) vector. The rotatory strength calculated in the velocity gauge formulation is indeed gauge-origin independent, as shown in Table 3, while the length gauge results are gauge-origin dependent.

As expected, the gauge-origin dependence of the rotatory strength calculated using the length gauge decreases when the basis set is extended.

4.2 Two-electron and one-electron spin-orbit operators in CPP calculations

As anticipated, the calculations with the full two-electron spin-orbit operator are time- and resource-consuming, and therefore we find it worthwhile to study how the use of approximate atomic-mean-field or effective-nuclear-charge spin-orbit (approximate) operators affects the calculated CPP intensities. For the rotational and dipole strength calculated for the HOMO-LUMO spin-forbidden transition in H_2O_2, the use of the approximate atomic mean-field spin-orbit coupling operator leads to results very similar to those yielded by the full two-electron operator, see Table 4. The effective charge operator exhibits a worse performance, albeit the results it yields are qualitatively correct.

This is, however, not the case when the transitions to (in spin-forbidden absorption) and from (in phosphorescence) the triplet π^* state in ketones are considered. As shown in Table 5, the rotational and dipole strengths calculated with the approximate operators (both AMFI-SO and EC-SO) are considerably underestimated in comparison with the values obtained using the full two-electron spin-orbit coupling operator (on the average, about halved). For sake of conciseness, Table 5 only shows the results for the absorption case, but a similar pattern is observed in the emission parameters.

Table 4 Comparison of the dipole [10^{-40} esu^2 cm^2] and rotational [10^{-40} esu cm erg G^{-1}] strengths (velocity gauge) of the spin-forbidden HOMO-LUMO transition in H_2O_2 calculated with different approximations of the spin-orbit operator. CAM-B3LYP results.

Basis	EC-SO	AMFI-SO	2e-SO
		Dipole strength, D	
aug-cc-pVDZ	4.94	3.82	3.85
d-aug-cc-pVQZ	4.50	3.81	3.63
		Rotational strength, $R \times 10^2$	
aug-cc-pVDZ	−1.94	−1.52	−1.52
d-aug-cc-pVQZ	−1.83	−1.56	−1.49

Table 5 Comparison of the dipole [10^{-40} esu^2 cm^2] and rotational [10^{-40} esu cm erg G^{-1}] strengths (velocity gauge) corresponding to the spin-forbidden $n \rightarrow \pi^*$ absorption in enones **1**-**4**, calculated with different approximations of the spin-orbit operator. CAM-B3LYP/aug-cc-pVDZ results.

Enone	EC-SO	AMFI-SO	2e-SO
		Dipole strength, D	
1	$1.86{\cdot}10^{-1}$	$1.42{\cdot}10^{-1}$	$3.51{\cdot}10^{-1}$
2	$5.91{\cdot}10^{-2}$	$6.42{\cdot}10^{-2}$	$1.14{\cdot}10^{-1}$
3	$1.74{\cdot}10^{-1}$	$1.35{\cdot}10^{-1}$	$3.31{\cdot}10^{-1}$
4	$8.3{\cdot}10^{-2}$	$6.36{\cdot}10^{-2}$	$1.54{\cdot}10^{-1}$
		Rotational strength, R	
1	$-2.24{\cdot}10^{-5}$	$-2.37{\cdot}10^{-5}$	$-4.94{\cdot}10^{-5}$
2	$-1.20{\cdot}10^{-4}$	$-1.42{\cdot}10^{-4}$	$-2.27{\cdot}10^{-4}$
3	$8.43{\cdot}10^{-5}$	$8.78{\cdot}10^{-5}$	$1.74{\cdot}10^{-4}$
4	$1.74{\cdot}10^{-5}$	$3.13{\cdot}10^{-5}$	$3.51{\cdot}10^{-5}$

Caution should therefore be exercised when using approximate forms of the spin-orbit operator, not only in calculations of CPP, but also of the phosphorescence lifetime (to which the dipole strength of the triplet-singlet transition is related).

4.3 β,γ-Enones

The optimized structures of the lowest triplet excited states (i.e., the ($n \rightarrow \pi^*$) transition) of the investigated β,γ-ketones are shown in Figures 2-5.

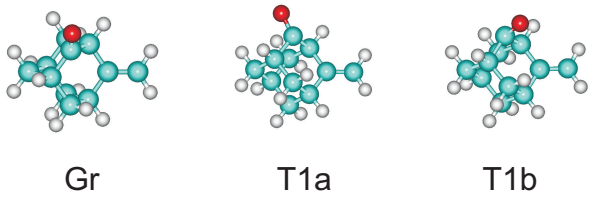

Fig. 2 The structure of the ground (Gr) and first triplet (T1) excited state of (1S,3R)-4-methyleneadamantan-2-one **1** (two stationary points on the triplet excited state PES).

Like in the corresponding singlet excited states,[2] the carbonyl group is no longer flat in the triplet states under study, and it inclines towards or away from the carbon-carbon double bond. This results in the appearance of two local minima on the excited state potential energy surface. As a consequence, the rotational strength of CPP (emission process) is vastly different from that of spin-forbidden ECD (absorption process). Moreover, the CPP intensities for the two minima on the triplet excited state potential energy surface have different sign (see Table 6), similar to what

Table 3 Gauge-origin dependence of rotational [10^{-40} esu cm erg G^{-1}] strengths in length gauge and velocity gauge formulations for the first, second and third transitions in H_2O_2. CM denotes gauge origin placed in the center of mass of H_2O_2, and CM+1 that it is moved by the (a_0,a_0,a_0) vector.

Basis set	Length		Velocity	
	CM	CM+1	CM	CM+1
aug-cc-pVDZ	$-1.025385\cdot 10^{-4}$	$-9.498249\cdot 10^{-5}$	$-1.234531\cdot 10^{-4}$	$-1.234530\cdot 10^{-4}$
aug-cc-pVTZ	$-1.078194\cdot 10^{-4}$	$-9.852125\cdot 10^{-5}$	$-1.202104\cdot 10^{-4}$	$-1.202103\cdot 10^{-4}$
aug-cc-pVQZ	$-1.124952\cdot 10^{-4}$	$-1.053031\cdot 10^{-4}$	$-1.225382\cdot 10^{-4}$	$-1.225383\cdot 10^{-4}$
aug-cc-pVDZ	$-1.437779\cdot 10^{-2}$	$-1.435351\cdot 10^{-2}$	$-1.523267\cdot 10^{-2}$	$-1.523268\cdot 10^{-2}$
aug-cc-pVTZ	$-1.471597\cdot 10^{-2}$	$-1.469452\cdot 10^{-2}$	$-1.476111\cdot 10^{-2}$	$-1.476111\cdot 10^{-2}$
aug-cc-pVQZ	$-1.490958\cdot 10^{-2}$	$-1.489075\cdot 10^{-2}$	$-1.472478\cdot 10^{-2}$	$-1.472479\cdot 10^{-2}$
aug-cc-pVDZ	$-1.614282\cdot 10^{-4}$	$-1.619254\cdot 10^{-4}$	$-9.393288\cdot 10^{-5}$	$-9.393376\cdot 10^{-5}$
aug-cc-pVTZ	$-1.744022\cdot 10^{-4}$	$-1.749018\cdot 10^{-4}$	$-1.418211\cdot 10^{-4}$	$-1.418207\cdot 10^{-4}$
aug-cc-pVQZ	$-1.916080\cdot 10^{-4}$	$-1.919585\cdot 10^{-4}$	$-1.680491\cdot 10^{-4}$	$-1.680489\cdot 10^{-4}$

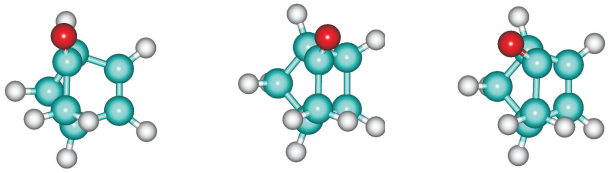

Fig. 3 The structure of the ground (Gr) and first triplet (T1) excited state of (1R,4R)-bicyclo[2.2.1]hept-5-en-2-one **2** (in both of them the carbonyl group is flat).

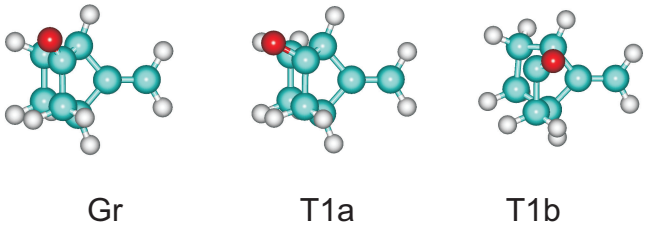

Fig. 4 The structure of the ground (Gr) and first triplet (T1) excited state of (1R)-7-methylenebicyclo[2.2.1]heptan-2-one **3** (two stationary points on the triplet excited state PES).

has been observed for singlet excited states. Thus, the sign of CPP signal can in principle be used to probe the structure of triplet excited states, in the same fashion as spin-allowed CPL is used to probe the structure of singlet excited states.

4.4 Ketones with conjugated double bonds

Two diketones in which the C=O bond is conjugated with another double bond have been studied in order to check how bond conjugation influences the structure of excited states resulting from the $n \rightarrow \pi^*$ transition, and consequently the CPP intensity. They are camphorquinone, **6** and its isomer **7**. In addition, the lowest-lying singlet and triplet excited state structures of an α,β-enone, namely the (R)-(−)4,4a,5,6,7,8-hexahydro-4a-methyl-2(3H)-naphthalenone **5**, have been optimized. In all three molecules the geometry optimization of singlet and triplet excited states resulted in flat structures of the carbonyl group, very similar to the ground state structures. The optimized structures of lowest triplet excited state are shown in Figure 6.

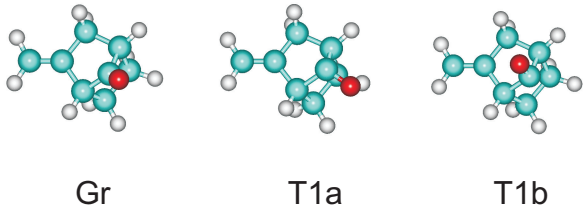

Fig. 5 The structure of the ground (Gr) and first triplet excited state (T1) of (1S)-2-methylenebicyclo[2.2.1]heptan-7-one **4** (two stationary points on the triplet excited state PES).

Table 6 The dipole [10^{-40} esu^2 cm^2] and rotational [10^{-40} esu cm erg G^{-1}] strengths of the β,γ-enones **1**, **2**, **3** and **4** corresponding to the transition to and from the T1 excited state (see Figures 2-5 for the structures). Velocity gauge, CAM-B3LYP/aug-cc-pVDZ results.

Strength	Gr	T1a	T1b
	Enone **1**		
D	$1.10\cdot 10^{-1}$	8.21	$2.00\cdot 10^{-1}$
R	$-2.53\cdot 10^{-4}$	$2.52\cdot 10^{-2}$	$-6.93\cdot 10^{-4}$
	Enone **2**		
D	$1.58\cdot 10^{-1}$	$1.50\cdot 10^{-1}$	$2.15\cdot 10^{-1}$
R	$2.32\cdot 10^{-5}$	$-1.99\cdot 10^{-4}$	$5.72\cdot 10^{-5}$
	Enone **3**		
D	$3.31\cdot 10^{-1}$	$3.80\cdot 10^{-1}$	$3.31\cdot 10^{-1}$
R	$1.68\cdot 10^{-4}$	$5.75\cdot 10^{-4}$	$1.68\cdot 10^{-4}$
	Enone **4**		
D	$1.58\cdot 10^{-1}$	$1.50\cdot 10^{-1}$	$2.15\cdot 10^{-1}$
R	$2.32\cdot 10^{-5}$	$-1.99\cdot 10^{-4}$	$5.72\cdot 10^{-5}$

The dipole and rotational strengths of the transitions to and from the three lowest singlet and triplet excited states of **6** and **7** (all corresponding to transitions within the O=C-C-C=O chromophore) are tabulated in Table 7. For camphorquinone **6**, the sign of the rotational strength in emission (for both spin-allowed and spin-forbidden transitions) is, as expected, the same as in absorption. For **7**, on the other hand, even though in all the excited states under study the carbonyl group is flat, the sign of the rotational strength varies in some cases (S3, T1) in the emission and absorption spectra. Thus, the sign change between circular dichroism and the corresponding CPL (or CPP) signal of a ketone does not necessarily indicate a distortion in the carbonyl group.

Table 7 The rotational strength R [10^{-40} esu cm erg G^{-1}] corresponding to the transitions to (absorption) and from (emission) the three lowest singlet (label S) and triplet (label T) excited states in 1,7,7-trimethylbicyclo[2.2.1]heptane-2,3-dione (e.g., camphorquinone) **6** and in (1S,4R,5R)-5,7,7-trimethylbicyclo[2.2.1]heptane-2,3-dione **7**. Velocity gauge, CAM-B3LYP/aug-cc-pVDZ results

Excited state	Absorption (CD)	Emission (CPL)	Excited state	Absorption (spin-forbidden CD)	Emission (CPP)
			6		
S1	0.99	1.43	T1	$-1.30\cdot10^{-6}$	$-3.10\cdot10^{-6}$
S2	−0.82	−0.87	T2	$7.14\cdot10^{-5}$	$6.12\cdot10^{-3}$
S3	6.58	29.96	T3	$-7.23\cdot10^{-4}$	$-7.33\cdot10^{-4}$
			7		
S1	−1.31	−0.69	T1	$-1.68\cdot10^{-5}$	$4.14\cdot10^{-6}$
S2	1.93	0.45	T2	$-1.49\cdot10^{-5}$	$-1.27\cdot10^{-4}$
S3	−11.41	0.97	T3	$1.68\cdot10^{-3}$	$2.59\cdot10^{-4}$

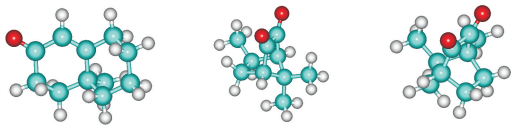

5 **6** **7**

Fig. 6 The equilibrium structure of the first triplet excited state of (R)-(−)4,4a,5,6,7,8-hexahydro-4a-methyl-2(3H)-naphthalenone (**5**), (1S,4R)-1,7,7-trimethylbicyclo[2.2.1]heptane-2,3-dione (**6**), and (1S,4R,5R)-5,7,7-trimethylbicyclo[2.2.1]heptane-2,3-dione (**7**).

The same is observed in the case of the lowest-lying triplet excited state of the α,β-enone **5** with conjugated C=O and C=C bonds. Even though in both ground and excited state the carbonyl group is flat, the rotational strengths in absorption and emission are almost exactly opposite: $-3.37\cdot10^{-43}$ Fr cm erg G^{-1} and $4.31\cdot10^{-43}$ Fr cm erg G^{-1}, respectively. Apparently, other subtle structural factors, such as for example the C=O bond length, influence significantly the value of the rotational strength.

5 Conclusions

We presented and discussed the methodology to calculate the intensity of circular dichroism in spin-forbidden absorption and of circularly polarized phosphorescence (CPP) signals, a manifestation of the optical activity of triplet-singlet transitions in chiral compounds. The expressions, developed within the framework of the response function formalism, rely on the evaluation of the magnetic dipole and electric dipole transition moments perturbed by spin-orbit coupling from the single residues of appropriate quadratic response functions.

TD-DFT calculations for H_2O_2 and a selected β,γ-enone have been carried out to test basis set convergence and the effect of moving the gauge origin on the spin-forbidden rotational strength in the length and velocity gauge formulations. It has been shown that the formulation is fairly robust, and that a somewhat faster basis set convergence is observed for the gauge-origin invariant velocity form. Another set of test calculations have been performed to check the performance of the approximate atomic mean field and effective nuclear charge spin-orbit operators, in place of the Breit-Pauli two-electron operator in calculations of CPP. It has been shown that the use of approximate operators can lead to underestimated transition moments.

The circularly polarized phosphorescence intensity has been calculated for valence $n \leftarrow \pi^*$ transitions in a selection of chiral enones and diketones. It appears that CPP is a sensitive probe of triplet excited state structure. For the β,γ-enones under investigation puckering of the carbonyl group in the $n \leftarrow \pi^*$ results in the presence of two minima on the lowest triplet excited state potential energy surface. The CPP signal has opposite sign for transitions to (from) the two different minima. Ketones with conjugated double bonds (a β,γ-enone and two 1,2-diones) exhibit undistorted low-lying excited states (singlet or triplet). However, even for them, a sign change between spin-forbidden circular dichroism signal and some of the CPP signals associated with emission from selected low-lying triplet states is predicted.

Acknowledgments

This work received support from the Polish National Science Center (Grant No. 2012/05/B/ST4/01236) and from the Wrocław Centre for Networking and Supercomputing and the Norwegian Supercomputing Program (Grant No. NN4654K) through grants of computer time. Support from the COST-CMTS Action CM1002 "COnvergent Distributed Environment for Computational Spectroscopy (CODECS)" is also acknowledged.

Appendix: units and conversion factors

In order to convert the dipole strength from atomic units to esu^2 (Fr^2 cm^2) and the rotational strength from atomic units to esu×emu (Fr cm erg G^{-1}) we have used following conversion factors, based on the CODATA 2010 compilation:[39]

- 1 au of dipole strength ($e^2a_0^2$) = 6.46048×10^{-36} Fr^2 cm^2
- 1 au of rotational strength ($\frac{e^2\hbar^2a_0}{m_e}$) = 4.71444×10^{-38} Fr cm erg G^{-1}

References

1 B. Pritchard and J. Autschbach, *ChemPhysChem*, 2010, **11**, 2409–2415.

2 M. Pecul and K. Ruud, *Phys. Chem. Chem. Phys.*, 2011, **11**, 643–650.

3 E. Castiglioni, S. Abbate and G. Longhi, *Appl. Spectrosc.*, 2010, **64**, 1416–1419.

4 S. Abbate, G. Longhi, F. Lebon, E. Castiglioni, S. Superchi, L. Pisani, F. Fontana, F. Torricelli, T. Caronna, C. Villani, R. Sabia, M. Tommasini, A. Lucotti, D. Mendola, A. Mele and D. A. Lightner, *J. Phys. Chem.* **C**, 2014, **118**, 1682–1695.

5 G. Longhi, S. Abbate, G. Mazzeo, E. Castiglioni, P. Mussini, T. Benincori, R. Martinazzo and F. Sannicolò, *J. Phys. Chem.* **C**, 2014, **118**, 16019–16027.

6 N. Steinberg, A. Gafni and I. Z. Steinberg, *J. Am. Chem. Soc.*, 1981, **103**, 1636–1640.

7 P. M. L. Blok, H. J. C. Jacobs and H. P. J. M. Dekkers, *J. Am. Chem. Soc.*, 1991, **113**, 794–801.

8 C. Shen, E. Anger, M. Srebro, N. Vanthuyne, K. K. Deol, T. D. Jefferson, G. Muller, J. A. G. Williams, L. Toupet, C. Roussel, J. Autschbach, R. Reau and J. Crassous, *Chem. Sci.*, 2014, **5**, 1915–1927.

9 N. Saleh, B. Moore, M. Srebro, N. Vanthuyne, L. Toupet, J. A. G. Williams, C. Roussel, K. K. Deol, G. Muller, J. Autschbach and J. Crassous, *Chemistry - A European Journal*, 2015, **21**, 1673–1681.

10 S. Kaizaki, J. Hidaka and Y. Shimura, *Inorg. Chem.*, 1973, **12**, 142–150.

11 S. F. Mason and B. J. Peart, *J. Chem. Soc., Dalton Trans.*, 1977, 937–941.

12 S. Kaizaki, J. Hidaka and Y. Shimura, *Inorg. Chem.*, 1985, **24**, 2080–2088.

13 J. A. Schaurte, D. G. Steel and A. Gafni, *Proc. Natl. Acad. Sci. U S A*, 1992, **89**, 10154–10158.

14 J. B. A. Ross, W. R. Laws, K. W. Rouslang and H. R. Wyssbrod, in *Tyrosine fluorescence and phosphorescence from protein and polypeptides*, ed. J. R. Lakowich, Plenum press, New York, 1992, vol. 3, ch. Biochemical applications, pp. 1–63.

15 O. Vahtras, H. Ågren, P. Jørgensen, H. J. A. Jensen, T. Helgaker and J. Olsen, *J. Chem. Phys.*, 1992, **97**, 9178–9187.

16 I. Tunell, Z. Rinkevicius, O. Vahtras, P. Sałek, T. Helgaker and H. Ågren, *J. Chem. Phys.*, 2003, **119**, 11024.

17 P. H. Schippers, J. P. M. van der Ploeg and H. P. J. M. Dekkers, *J. Am. Chem. Soc.*, 1983, **105**, 84.

18 J. Olsen and P. Jørgensen, *J. Chem. Phys.*, 1985, **82**, 3235.

19 K. L. Bak, A. E. Hansen, K. Ruud, T. Helgaker, J. Olsen and P. Jørgensen, *Theor. Chim. Acta*, 1995, **90**, 441.

20 T. Saue and H. Jensen, *J. Chem. Phys.*, 2003, **118**, 522.

21 E. Jansson, P. Norman, B. Minaev and H. Ågren, *J. Chem. Phys.*, 2006, **124**, 114106.

22 M. Jaszunski, A. Rizzo and K. Ruud, *Handbook of Computational Chemistry*, Springer Science (in two volumes) + Business Media (in three volumes), 2012, vol. 1, ch. 11, pp. 361–441.

23 B. A. Hess, C. M. Marian, U. Wahlgren and O. Gropen, *Chem. Phys. Lett.*, 1996, **251**, 365.

24 C. M. Marian and U. Wahlgren, *Chem. Phys. Lett.*, 1996, **251**, 357.

25 S. Koseki, M. S. Gordon, M. W. Schmidt and N. Matsunaga, *J. Phys. Chem.*, 1995, **99**, 12764.

26 F. J. Neese, *J. Chem. Phys.*, 2005, **122**, 034107.

27 B. Schimmelpfennig, 1996, AMFI - an atomic mean field integral program. University of Stockholm, Stockholm, Sweden.

28 S. Koseki, M. W. Schmidt and M. S. Gordon, *J. Phys. Chem.*, 1992, **96**, 10768–10772.

29 T. Yanai, D. P. Tew and N. C. Handy, *Chem. Phys. Lett.*, 2004, **91**, 551.

30 T. H. Dunning, *J. Chem. Phys.*, 1989, **90**, 1007.

31 R. A. Kendall, T. H. Dunning and R. J. Harrison, *J. Chem. Phys.*, 1992, **96**, 6796.

32 D. E. Woon and T. H. Dunning, *J. Chem. Phys.*, 1993, **98**, 1358.

33 D. E. Woon and T. H. Dunning, *J. Chem. Phys.*, 1994, **100**, 2975.

34 Dalton, a Molecular Electronic Structure Program, Release Dalton2015.0 (2015), see http://daltonprogram.org/.

35 K. Aidas, C. Angeli, K. L. Bak, V. Bakken, R. Bast, L. Boman, O. Christiansen, R. Cimiraglia, S. Coriani, P. Dahle, E. Dalskov, U. Ekström, T. Enevoldsen, J. J. Eriksen, P. Ettenhuber, B. Fernández, L. Ferrighi, H. Fliegl, L. Frediani, K. Hald, A. Halkier, C. Hättig, H. Heiberg, T. Helgaker, A. C. Hennum, H. Hettema, E. Hjertenaes, S. Høst, I.-M. Høyvik, M. F. Iozzi, B. Jansík, H. Jensen, D. Jonsson, P. Jørgensen, J. Kauczor, S. Kirpekar, T. Kjaergaard, W. Klopper, S. Knecht, R. Kobayashi, H. Koch, J. Kongsted, A. Krapp, K. Kristensen, A. Ligabue, O. Lutnæs, J. Melo, K. Mikkelsen, R. Myhre, C. Neiss, C. Nielsen, P. Norman, J. Olsen, J. Olsen, A. Osted, M. Packer, F. Pawlowski, T. Pedersen, P. Provasi, S. Reine, Z. Rinkevicius, T. A. Ruden, K. Ruud, V. V. Rybkin, P. Salek, C. C. M. Samson, A. S. de Merás, T. Saue, S. Sauer, B. Schimmelpfennig, K. Sneskov, A. H. Steindal, K. O. Sylvester-Hvid, P. R. Taylor, A. M. Teale, E. I. Tellgren, D. P. Tew, A. J. Thorvaldsen, L. Thø gersen, O. Vahtras, M. A. Watson, D. J. D. Wilson, M. Ziolkowski and H. Ågren, *WIREs Comput. Mol. Sci.*, 2014, **4**, 269–284.

36 S. Coriani, M. Pecul, A. Rizzo, P. Jørgensen and M. Jaszuński, *J. Chem. Phys.*, 2002, **117**, 6417.

37 J. G. Hill and G. Bucher, *J. Phys. Chem.* **A**, 2014, **118**, 2332–2343.

38 M. Pecul, K. Ruud and T. Helgaker, *Chem. Phys. Lett.*, 2004, **388**, 110.

39 P. J. Mohr, B. N. Taylor and D. B. Newell, *Rev. Mod. Phys.*, 2012, **84**, 1527.